Supporting Information

Optimization of Electron Transfer Pathways in Atomically Precise Metal Nanoclusters: Catalyzing a Leap in Solar Water Oxidation

Peng Su[a], Jialiang Liu[a], Fang-Xing Xiao[a, b*]

a. College of Materials Science and Engineering, Fuzhou University, New Campus, Minhou, Fujian Province, 350108, China.

b. State Key Laboratory of Structural Chemistry, Fujian Institute of Research on the Structure of Matter, Chinese Academy of Sciences, Fuzhou, Fujian 350002, PR China.

E-mail: fxxiao@fzu.edu.cn

Table of Contents

Page NO.

Experimental section

1. Materials

Titanium sheet (99.99%, 0.1×20×50 mm), Graphite sheet (99.6%), Deionized water (DI H_2O, Millipore, 18.2 MΩ cm resistivity), Ethylene glycol ($C_2H_6O_2$), Ammonia fluoride (NH_4F), Hydrogen fluoride (HF), Nitric acid (HNO_3), Sodium hydroxide (NaOH), Sodium sulfate (Na_2SO_4), hydrochloric acid (HCl), ammonium oxalate ($(NH_4)_2C_2O_4$), Sodium borohydride ($NaBH_4$), Silver nitrate ($AgNO_3$), gold (III) chloride trihydrate ($HAuCl_4 \cdot 3H_2O$) were obtained from Sinopharm Chemical Reagent Co., Ltd (Shanghai, China). Lglutathione (GSH) and poly(diallyl-dimethyl-ammonium chloride) solution (PDDA, average Mw 200.000-350.000) were obtained from Sigma-Aldrich. All reagents above were used as received without further purification.

2. Preparation of TNTA[1]

A secondary electrochemical anodization method was employed to prepare TiO_2 nanoarrays. Ti foil was first thoroughly sonicated in acetone, ethanol and DI H_2O for 15 min, respectively. Then, Ti sheets were immersed in a mixed solution of HF-HNO_3-H_2O with volume ratio of 1: 4: 5 for 20 s, washed by DI H_2O and dried with a gentle N_2 stream. Anodization was carried out under ambient conditions at 50 V for 2 h with ca. 3 cm separation distance between the working (Ti foil) and counter electrode (graphite). The electrolyte consists of 0.3 wt. % of NH_4F (0.6 g) in ethylene glycol (196 mL) and DI H_2O (4 mL). After the first-step anodization, the as-obtained TiO_2 layer was removed from Ti foil by sonication in ethanol for 5 min, washed by DI H_2O and dried with a N_2 stream. The second anodization was performed at 50 V for 30 min to produce the TNTAs. Similarly, the resulting TNTAs were also washed by DI H_2O, dried with a N_2 stream and finally calcined at 450°C for 3 h in air with a heating rate of 5 °C min^{-1}.

3. Preparation of Ag_x@GSH nanoclusters (Ag_x NCs)[2]

In brief, 12.5 mL of 20 mM $AgNO_3$ and 7.5 mL of 50 mM reduced glutathione (GSH) were added to a

500 mL flask containing 200 mL of deionized water. White precipitates appeared instantly as a result of the formation of Ag_x@GSH complexes, and this mixture was stirred for 2 min. The precipitates dissolved completely when the pH of the reaction mixture was changed to 11 by adding a 1 M NaOH solution, forming a transparent solution. Heating this solution at 90 °C (inside of solution) for 1 h under stirring at 500 rpm yielded initial products of Ag_x@GSH, whose differences were evident from the color change of the transparent solution to light orange. After the solution was naturally cooled to room temperature, the pH was changed again to 3.75 by adding 1 M HCl. This abrupt pH change resulted in an instantaneous darkening of the solution color that signified the aggregation of Ag thiolate complexes on the surface of the Ag core. The color of the NC solution became darker over time. Hence, the NC solution was aged for 24 h at room temperature to complete this process, and no further change in the color was observed after 24 h. Any precipitates formed during this period were removed via centrifugation. The Ag_x@GSH nanoclusters were collected without purification and stored at 4 °C for further characterization.

4. Preparation of $Ag_{16}(GSH)_9$ and $Ag_9(GSH)_6$ NCs[2]

Aqueous solutions of $AgNO_3$ (20 mM) and GSH (50 mM) were prepared with ultrapure water. An aqueous solution of $NaBH_4$ (112 mM) was freshly prepared by dissolving 43 mg of $NaBH_4$ in 2 mL of 1 M NaOH solution, followed by the addition of 8 mL of DI water. The addition of a certain amount of NaOH to the $NaBH_4$ solution was used to improve the stability of borohydride ions against hydrolysis. In a typical experiment to synthesize $Ag_{16}(GSH)_9$ and $Ag_9(GSH)_6$ NCs, aqueous solutions of $AgNO_3$ (125 μL, 20 mM) and GSH (150 μL, 50 mM) were first mixed in water (4.85 mL) S3 under vigorous stirring to form thiolate-Ag complexes, followed by the addition of an aqueous solution of $NaBH_4$ (50 μL, 112 mM). A deep-red solution of Ag NCs (~5mL) was collected after 5 min. This Ag NC solution was then incubated at room temperature for 3h, and the deep-red solution gradually decomposed into a colorless solution, leading to the formation of thiolate-Ag complexes. Subsequently, a certain amount of 112 mM $NaBH_4$ [50 μL for the

synthesis of $Ag_{16}(GSH)_9$ or 250 μL for $Ag_9(GSH)_6$ NCs] was introduced into this colorless solution under vigorous stirring, leading to the formation of a light-brown Ag NC solution after 15 min. Without stirring, this light-brown Ag NC solution was incubated at room temperature for a certain period of time [8 h for $Ag_{16}(GSH)_9$ and 48 h for $Ag_9(GSH)_6$ NCs]. A strong red or green emission was then observed in the aqueous phase. The $Ag_{16}(GSH)_9$ NCs (Ag_{16} NCs) or $Ag_9(GSH)_6$ NCs (Ag_{16} NCs) were collected without purification and stored at 4 °C for further characterization.

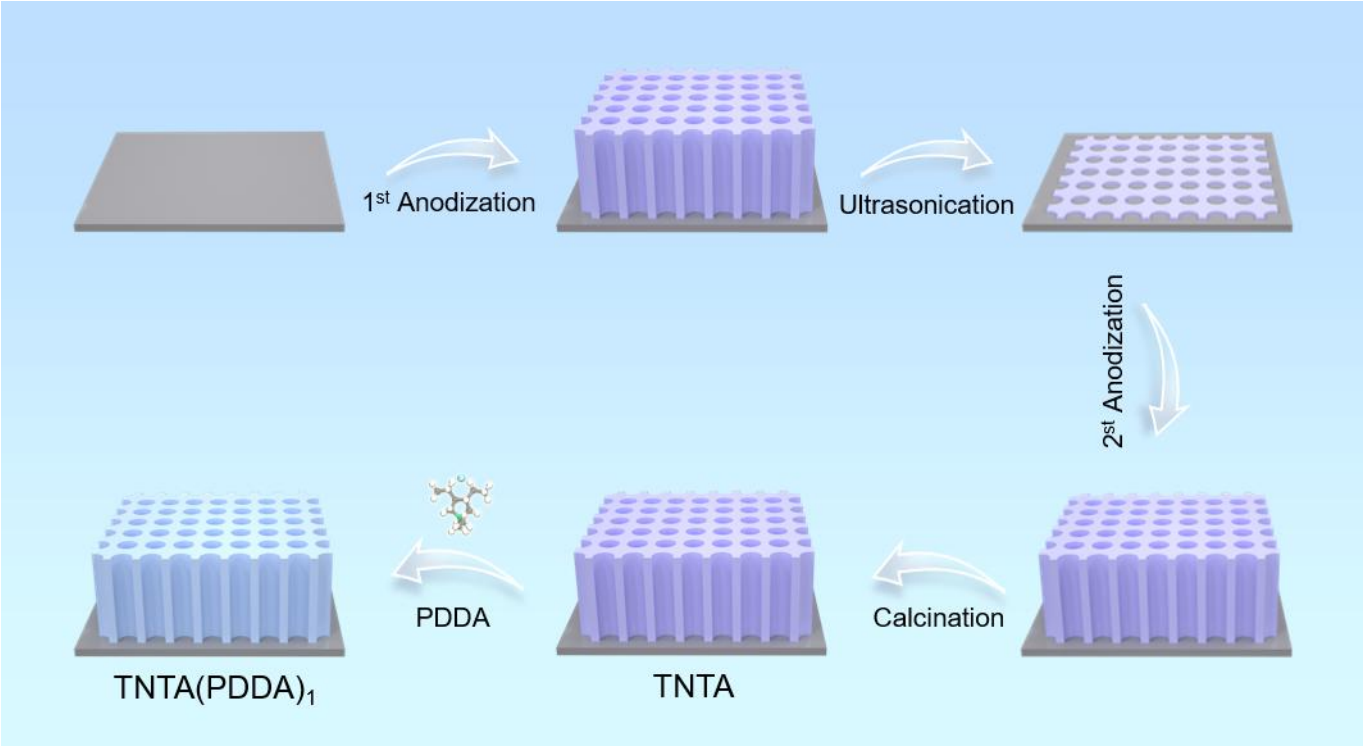

Figure S1. Schematic illustration for LbL assembly of TNTA/$(PDDA)_1$ multilayered heterostructure.

Note: TiO_2 nanotube array (TNTA) were fabricated using a two-step anodization method. Compared with single-step anodization, the core advantage of the two-step anodization method lies in its "sacrificial first, perfect later" preparation strategy. Specifically, the nanotube arrays generated in the first anodization process usually have poor orderliness. Subsequently, the TiO_2 layer is completely removed in ethanol by ultrasonication, thereby forming a porous oxide layer template with a certain degree of orderliness on the surface of the titanium sheet. Since this template provides a highly ordered pit structure, the second oxidation can be directly initiated at uniform and regular nucleation points, bypassing the random nucleation stage, and ultimately growing highly ordered and uniform TNTA.

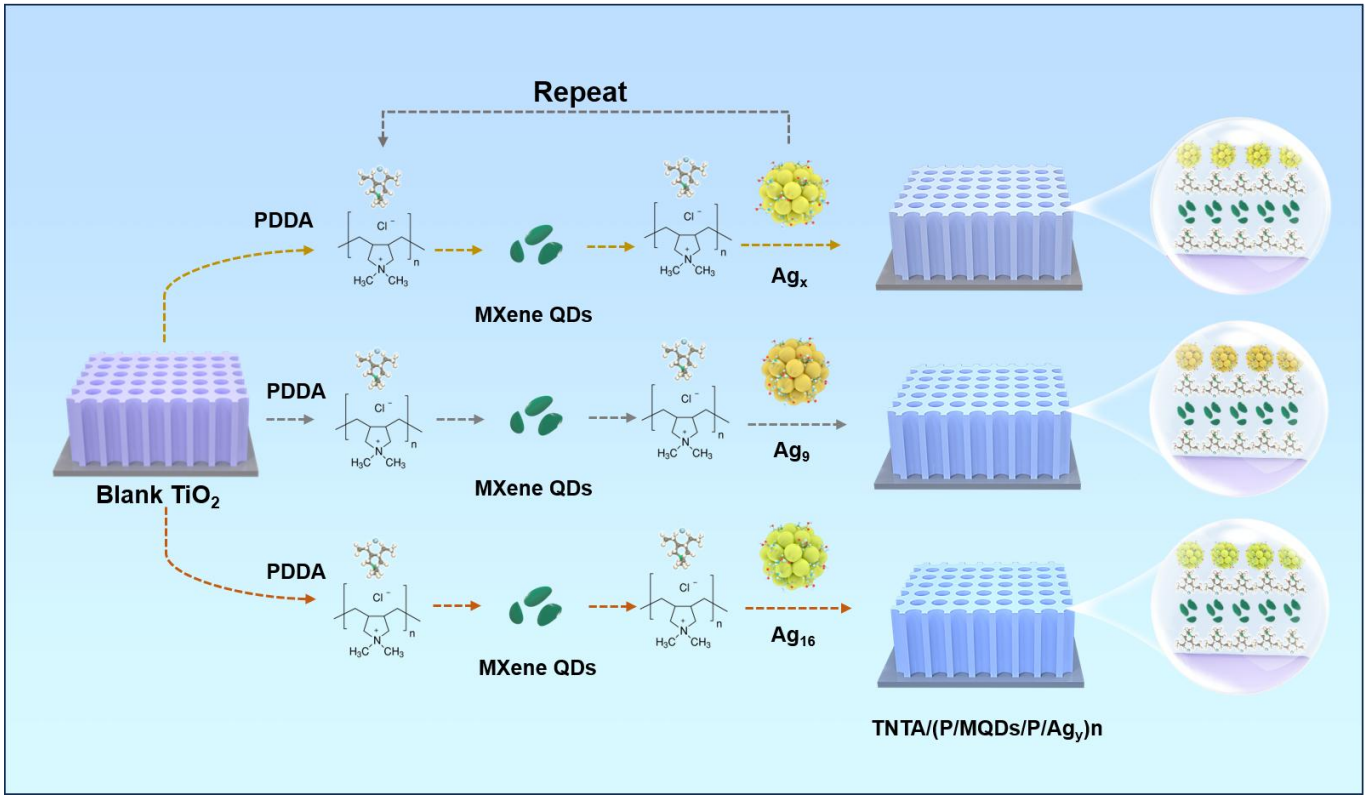

Figure S2. Schematic illustration for LbL assembly of TNTA/(P/MQDs/P/Ag$_y$)n (y = x, 9, 16) multilayered heterostructures.

Note: Through the layer-by-layer self-assembly technique, using positively charged PDDA, negatively charged MQDs, and negatively charged Ag$_x$@GSH as basic functional units, we have successfully constructed a structurally ordered multilayer heterojunction on the TNTA substrate. Moreover, this method demonstrates good versatility. Ag$_x$@GSH nanocrystals can be replaced by other silver nanoclusters (Ag$_9$(GSH)$_6$, Ag$_{16}$(GSH)$_9$), providing convenience for systematic studies on the effects of different components on the performance of photoanodes.

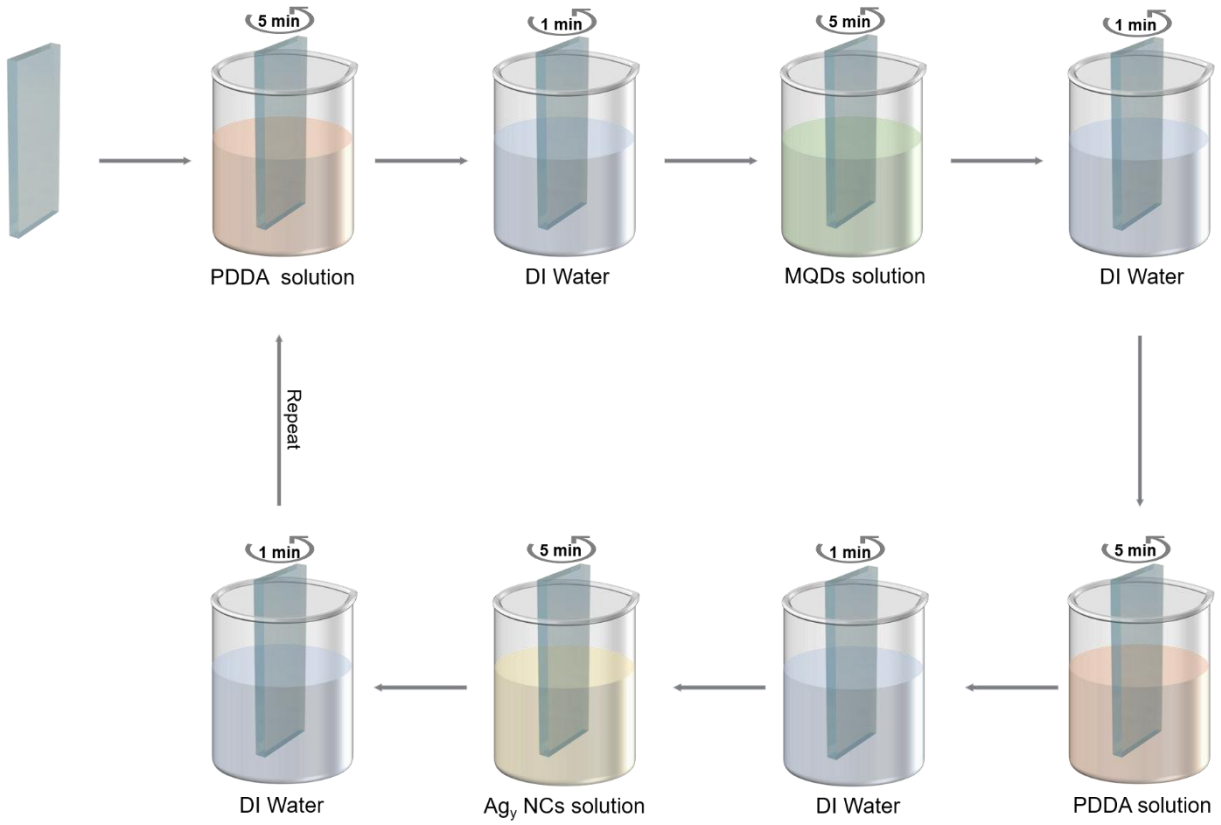

Figure S3. Schematic flowchart for LbL assembly of TNTA/(P/MQDs/P/Ag_y)$_n$.

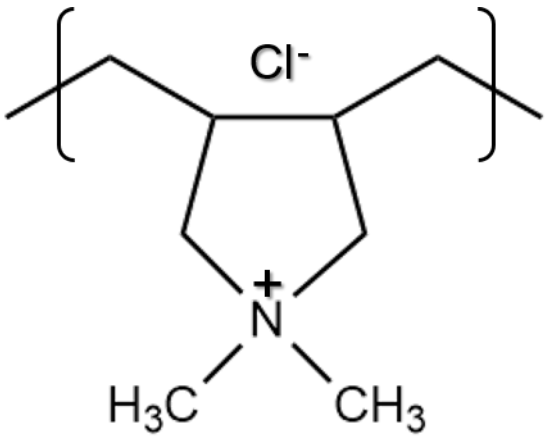

Figure S4. Molecular structure of PDDA.

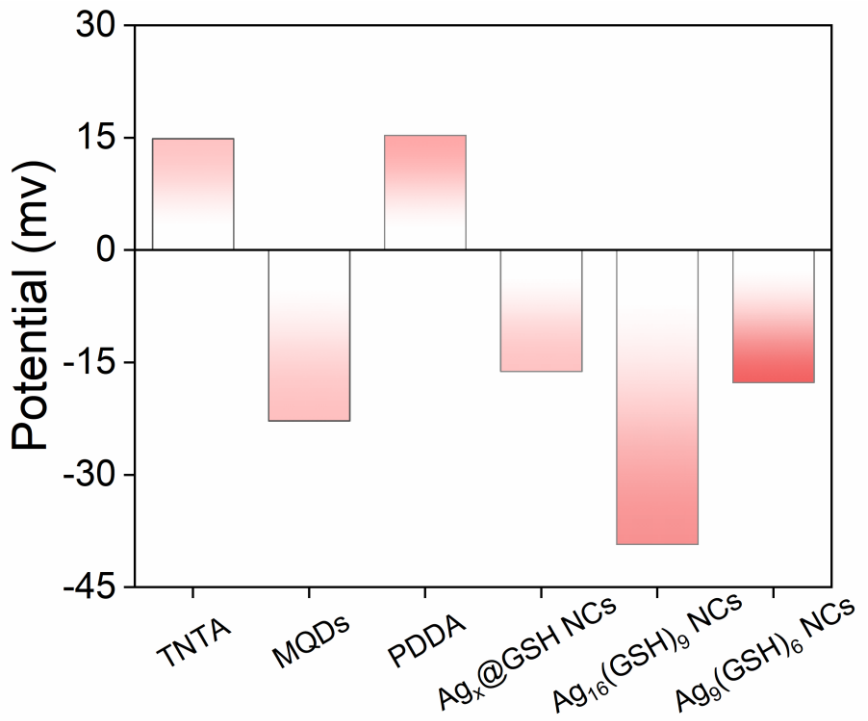

Figure S5. Zeta potentials of TNTA, MQDs, PDDA, Ag_x@GSH NCs, $Ag_9(GSH)_6$ NCs and $Ag_{16}(GSH)_9$ NCs.

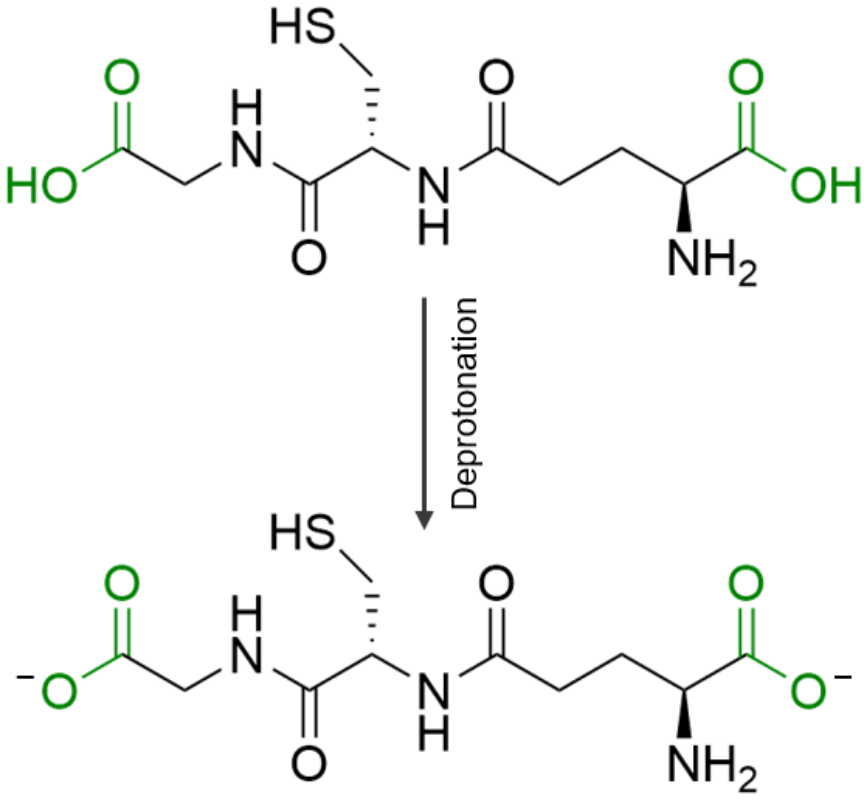

Figure S6. Molecular structure of GSH ligand along with deprotonation process.

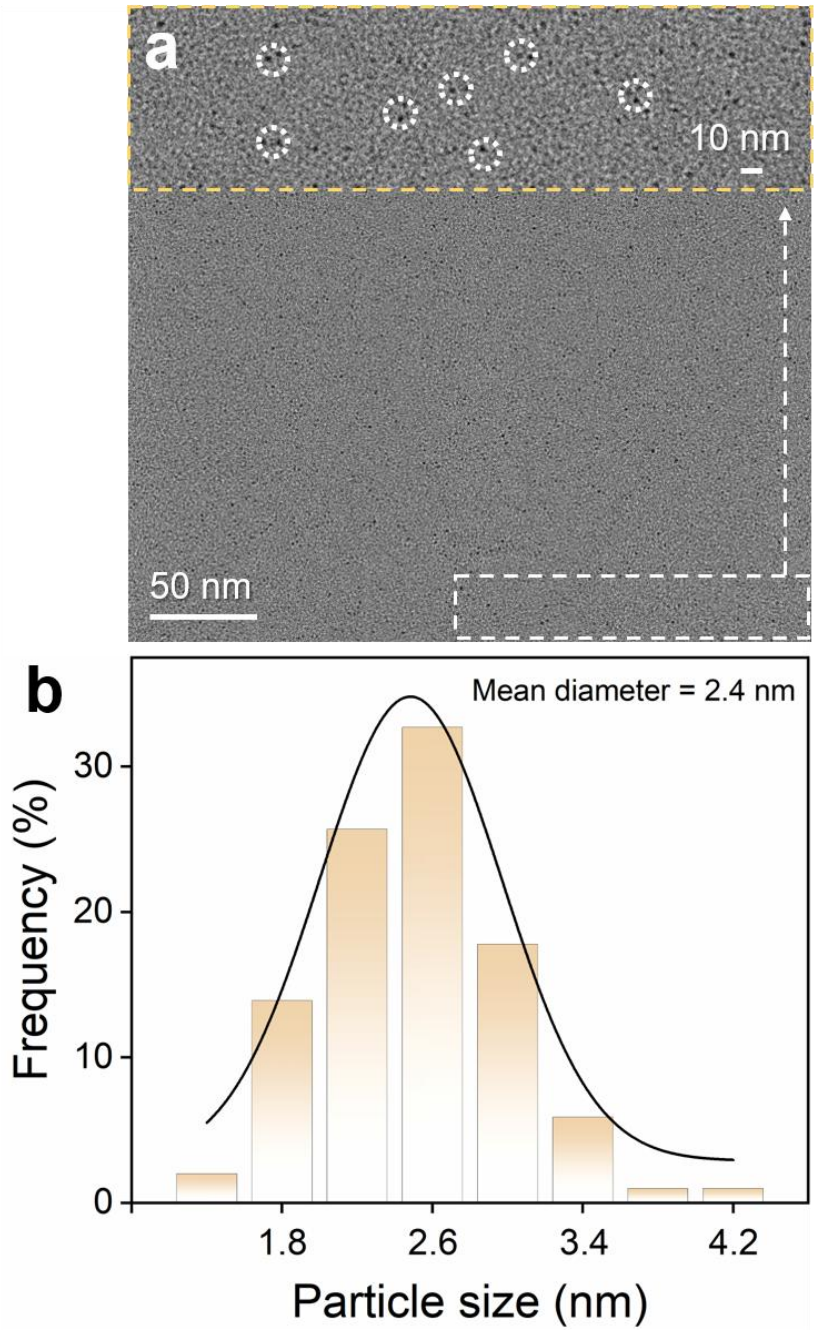

Figure S7. (a) TEM image and (b) size distribution histogram of Ag_x@GSH NCs.

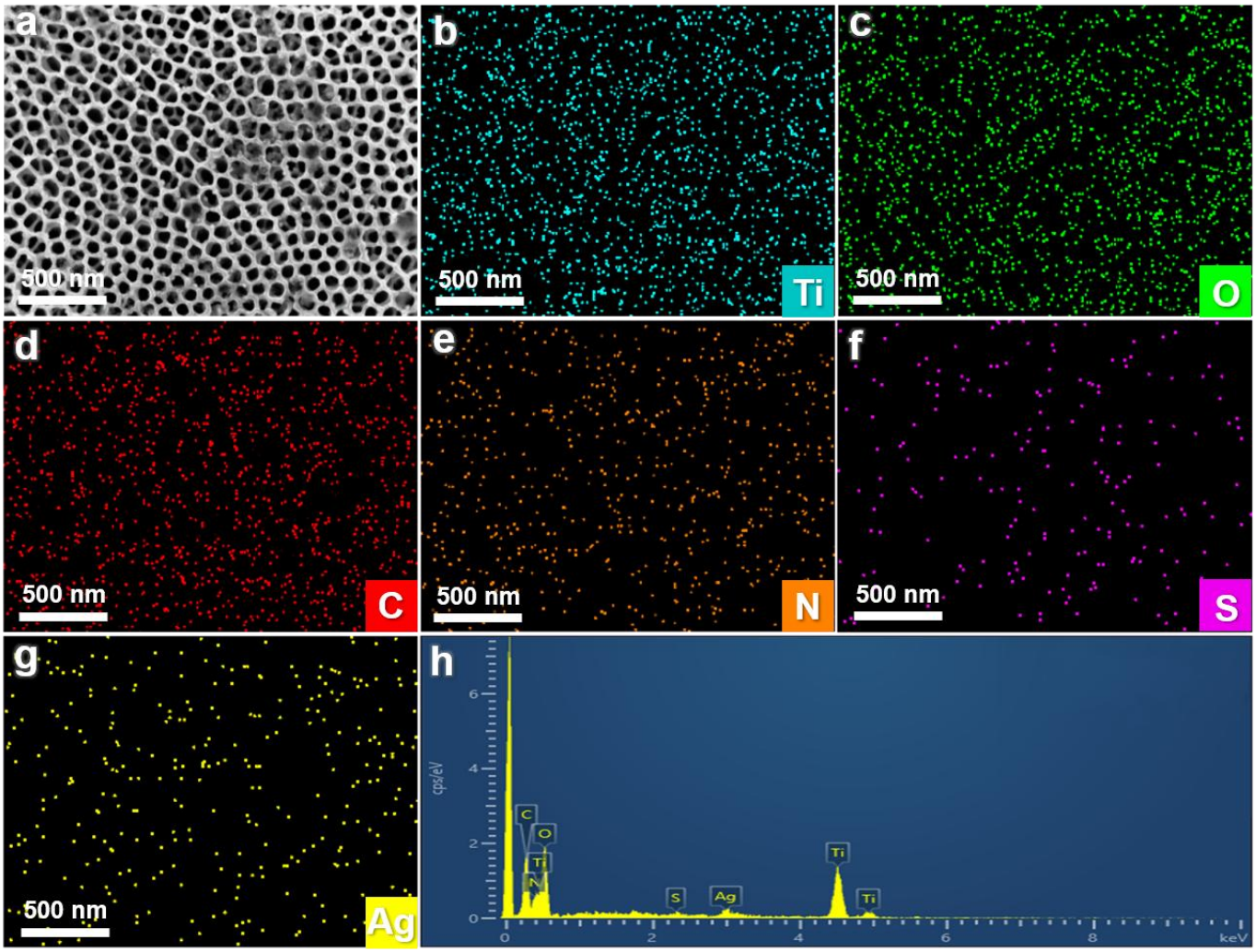

Figure S8. (a) Top-view SEM image of TNTA/$(Ag_x)_6$ with (b-g) elemental mapping and (h) EDS results.

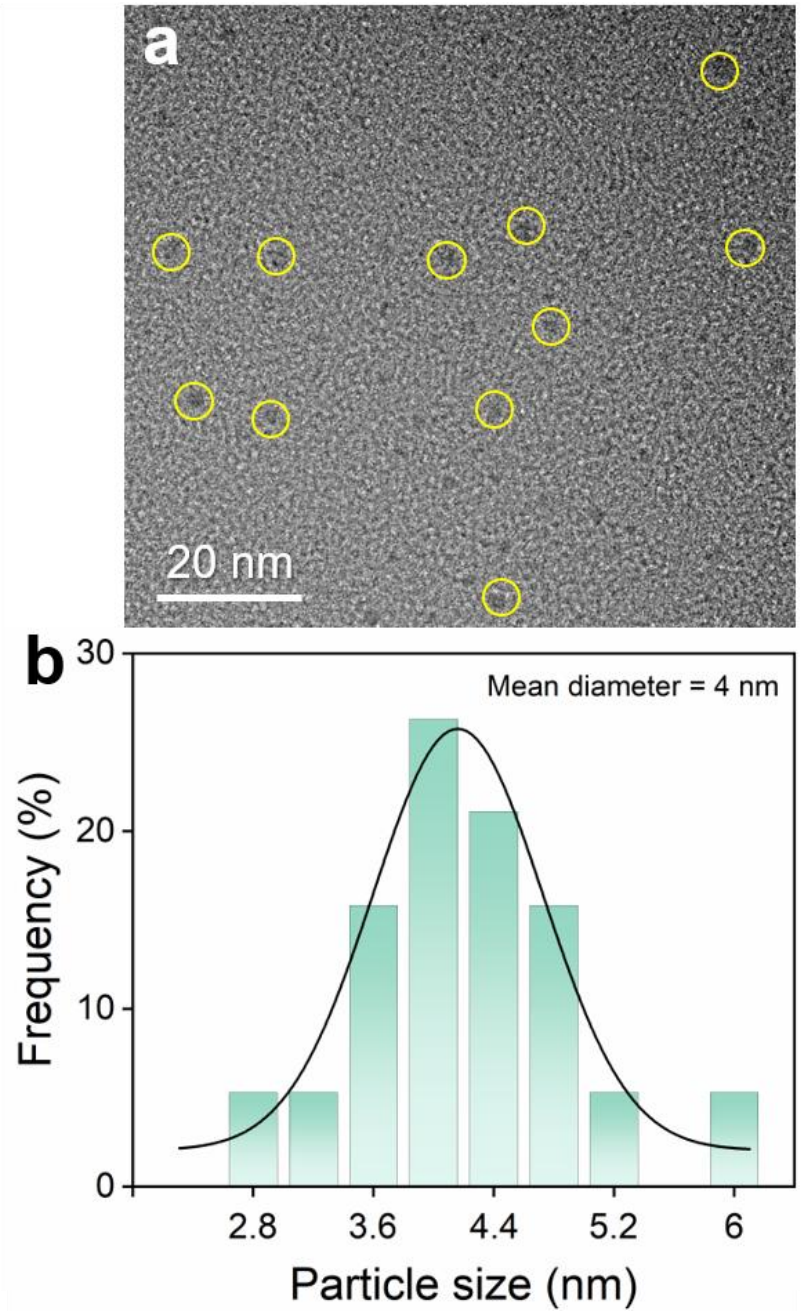

Figure S9. (a) TEM image and (b) size distribution histogram of MQDs.

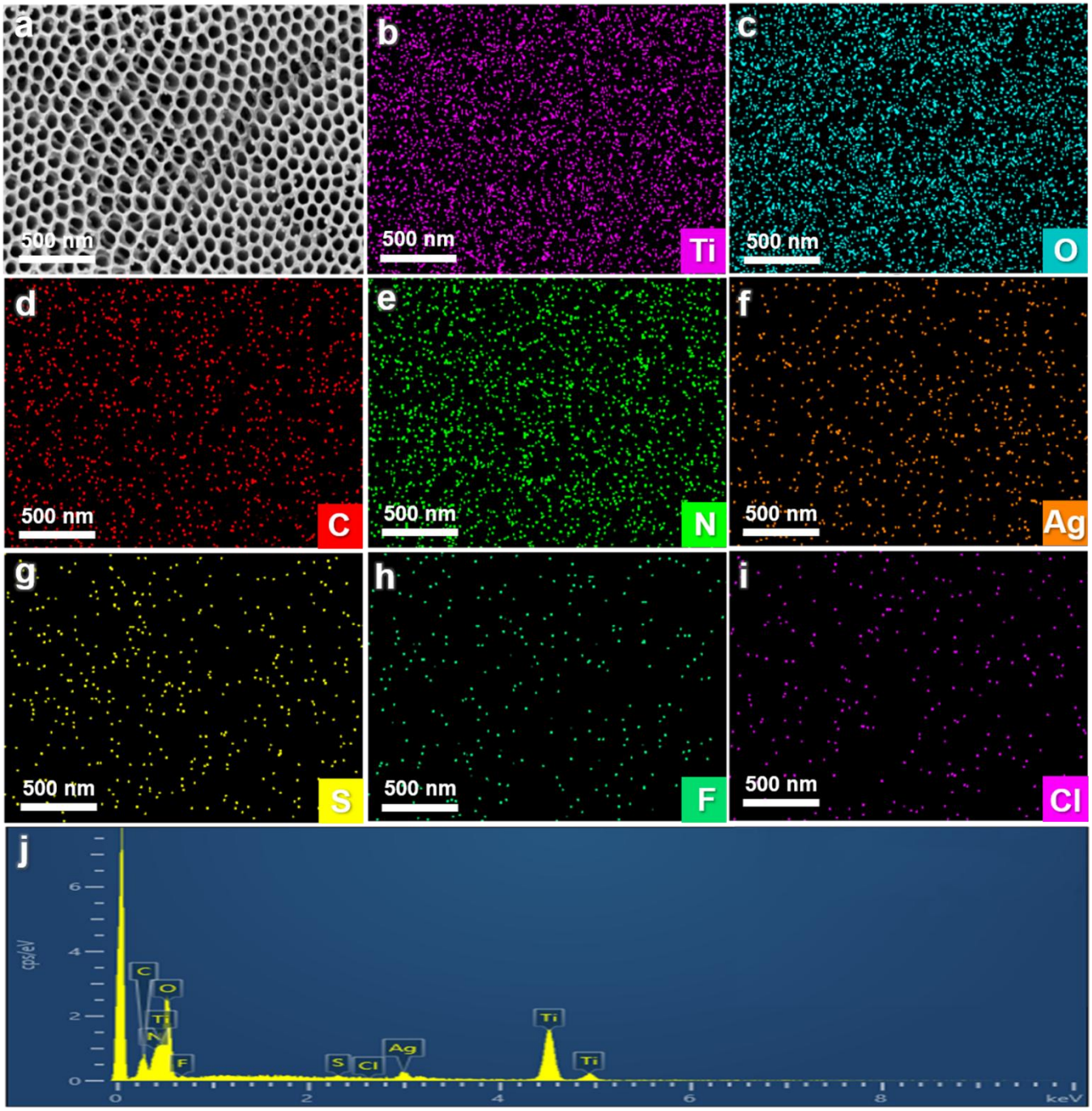

Figure S10. (a) Top-view SEM image of TNTA/(P/MQDs/P/Ag_x)$_6$ with (b-i) elemental mapping and (j) EDS results.

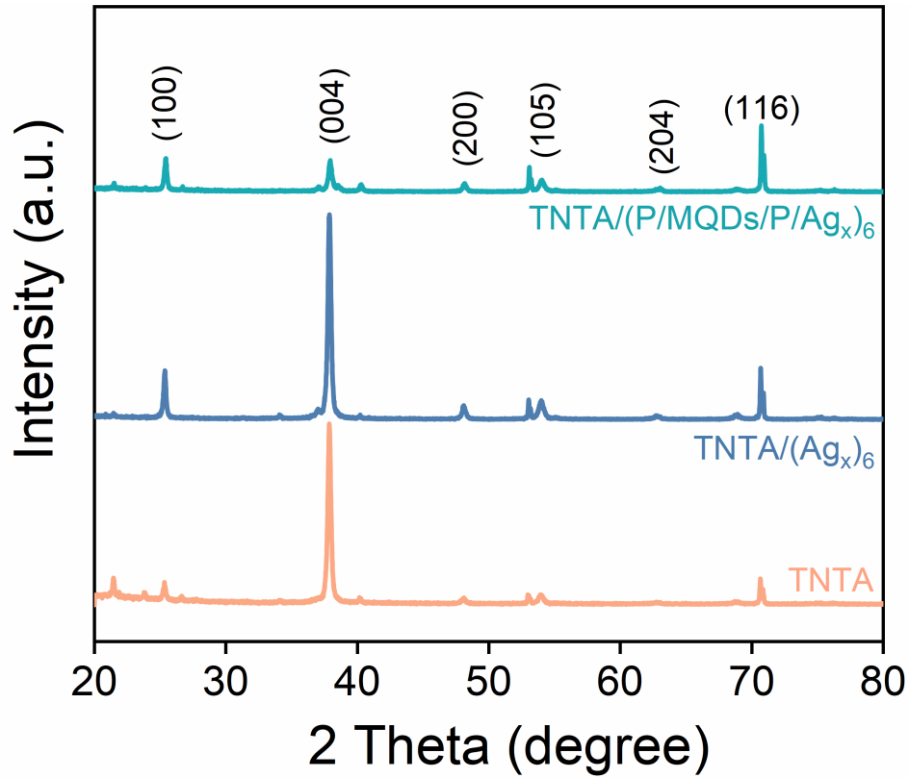

Figure S11. XRD results of TNTA, TNTA/(Ag$_x$)$_6$ and TNTA/(P/MQDs/P/Ag$_x$)$_6$.

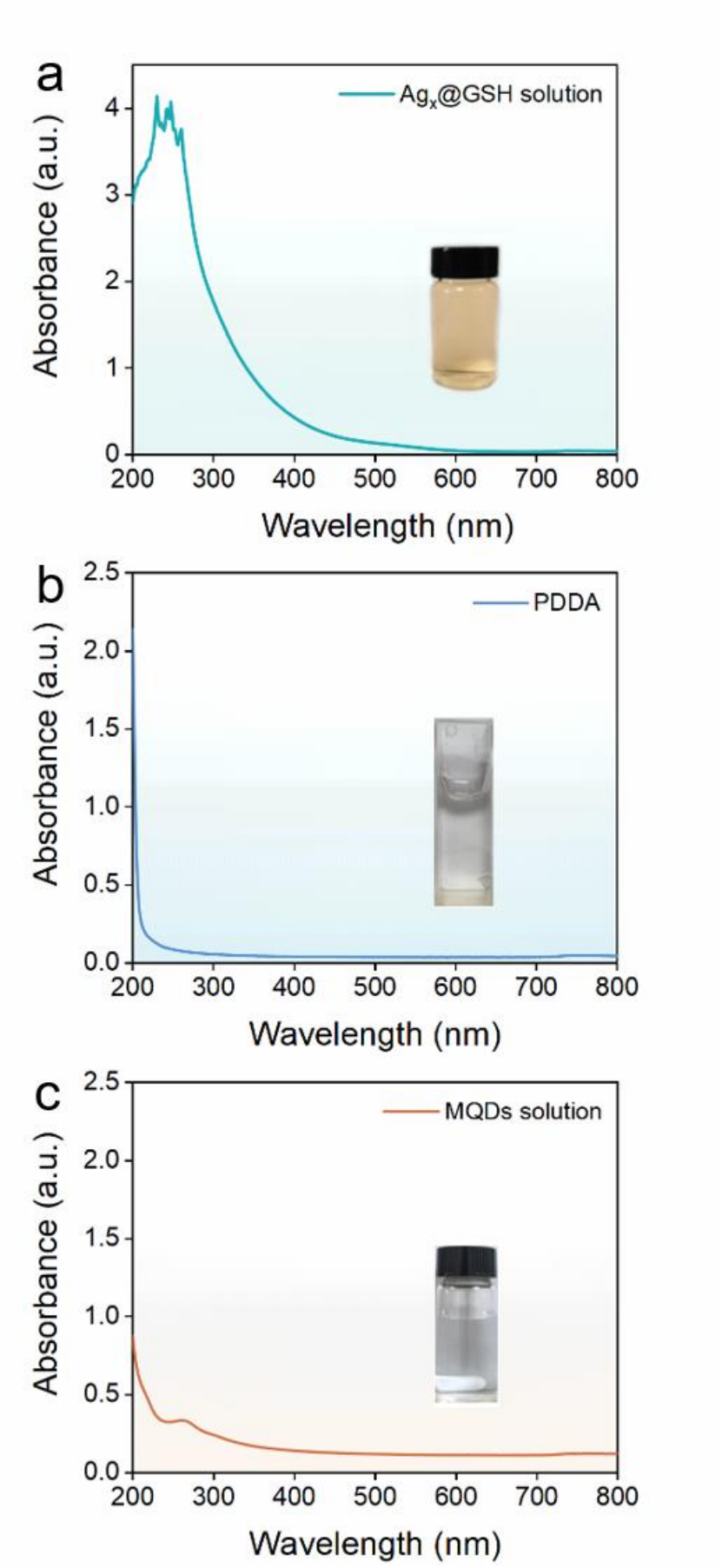

Figure S12. UV-vis absorption spectra of (a) Ag_x@GSH NCs, (b) PDDA and (c) MQDs solution.

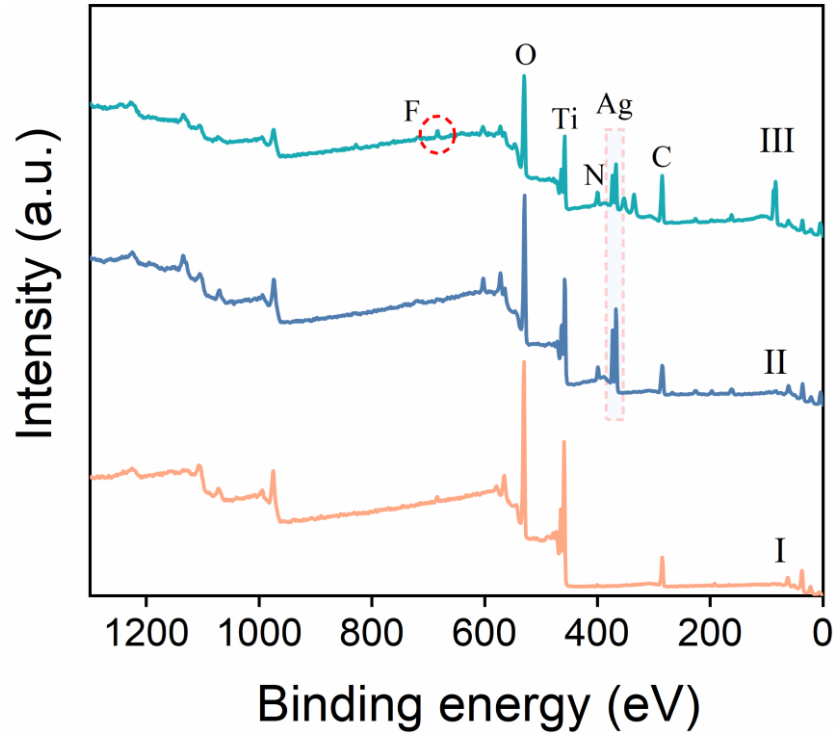

Figure S13. Survey spectra of (I) TNTA, (II) TNTA/$(Ag_x)_6$ and (III) TNTA/$(P/MQDs/P/Ag_x)_6$.

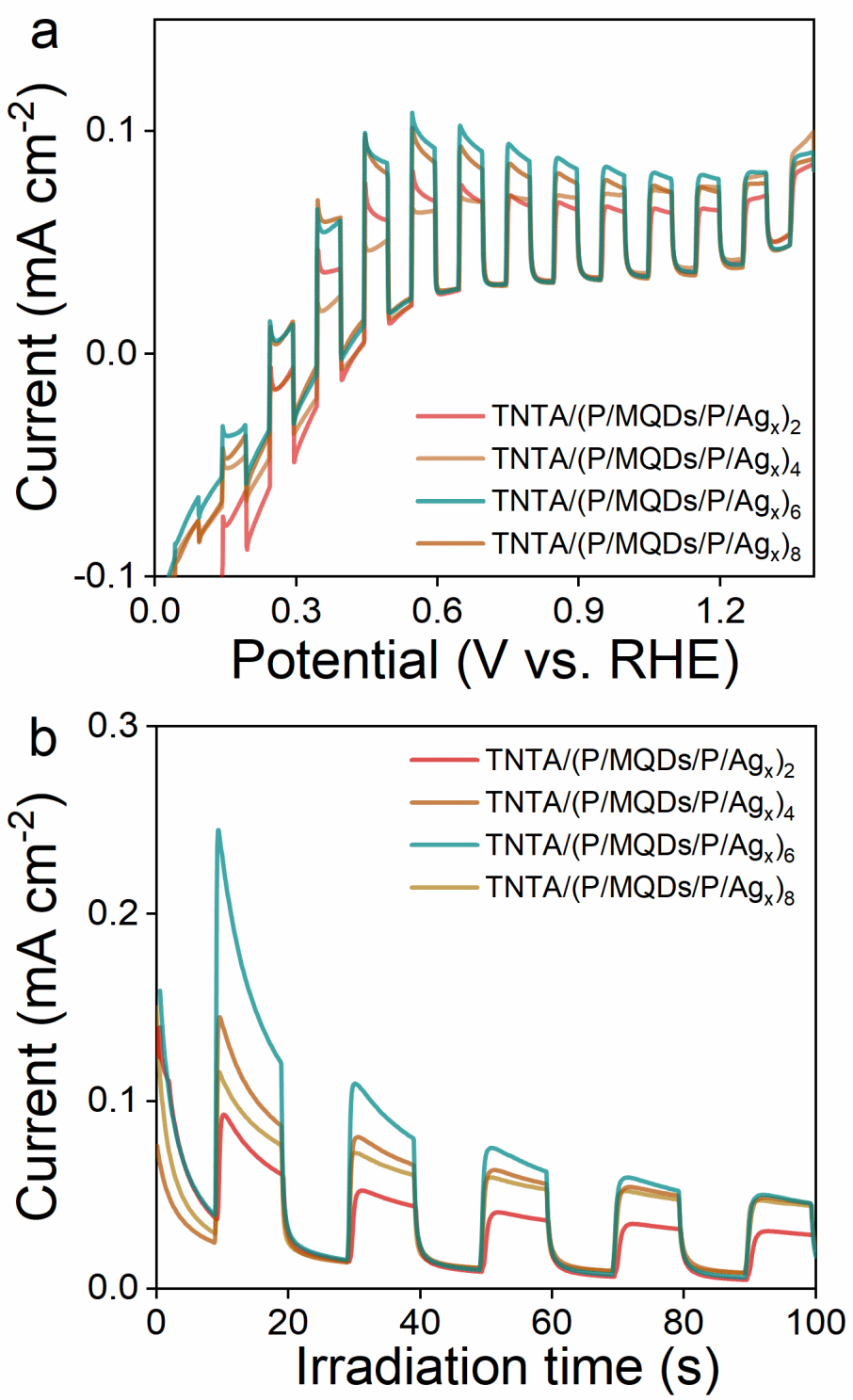

Figure S14. (a) LSV results and (b) I-t responses of TNTA/(P/MQDs/P/Ag_x)$_n$ (n = 2, 4, 6, 8).

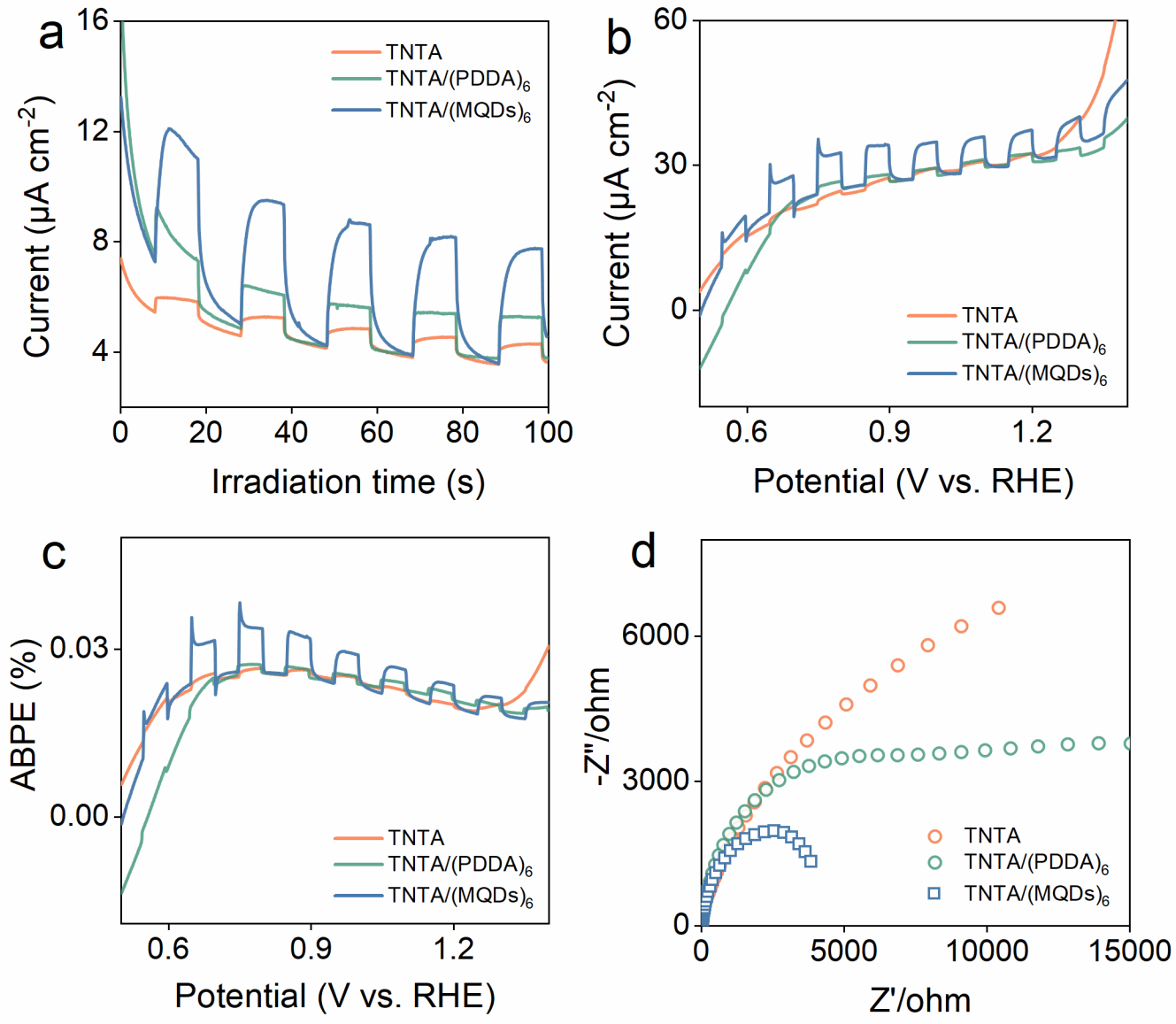

Figure S15. (a) I-t results (bias: 1.23 V vs. RHE, 0-100 s), (b) LSV, (c) ABPE and (d) EIS results of TNTA, TNTA/$(PDDA)_6$ and TNTA/$(MQDs)_6$.

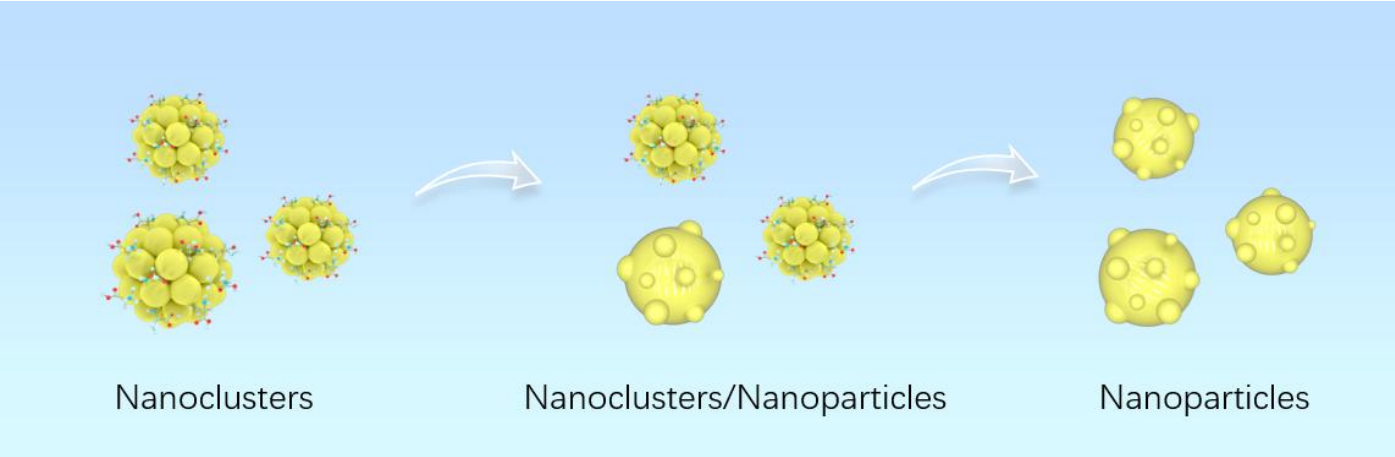

Figure S16. Schematic diagram depicting the mechanism for in-situ self-transformation of Ag_y NCs to Ag NPs.

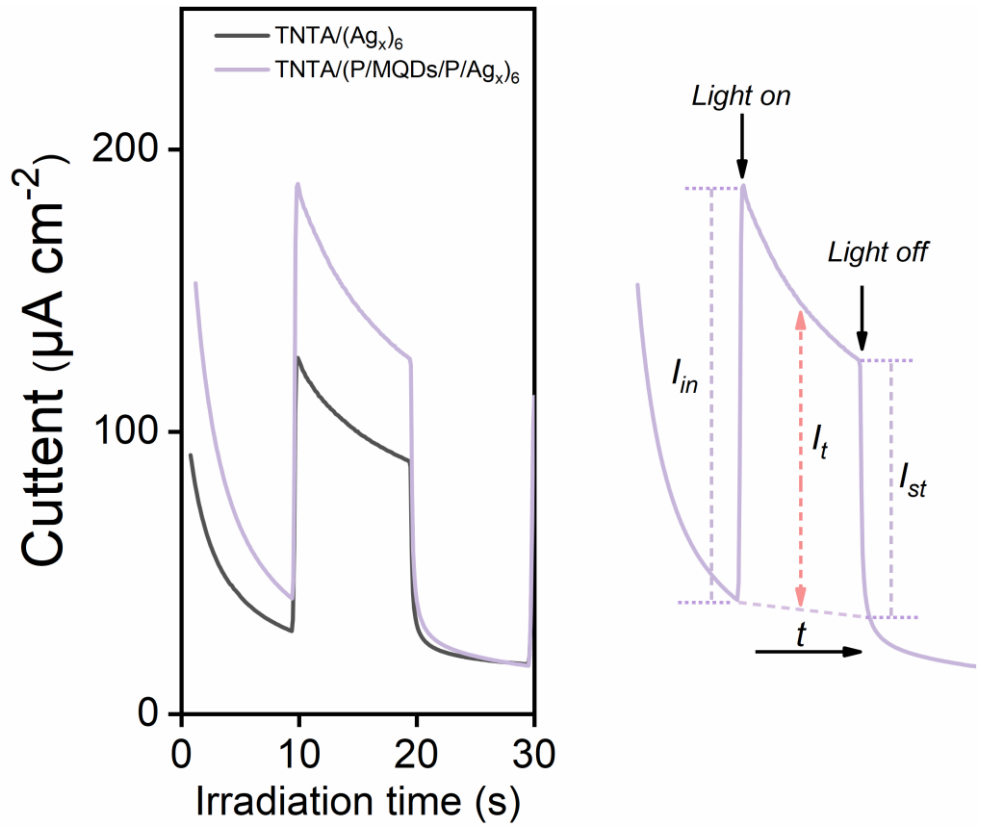

Figure S17. Photocurrent (bias: 1.0 V vs. RHE) of TNTA/(P/MQDs/P/Ag$_x$)$_6$ and TNTA/(Ag$_x$)$_6$ under visible light (λ ＞420 nm) irradiation.

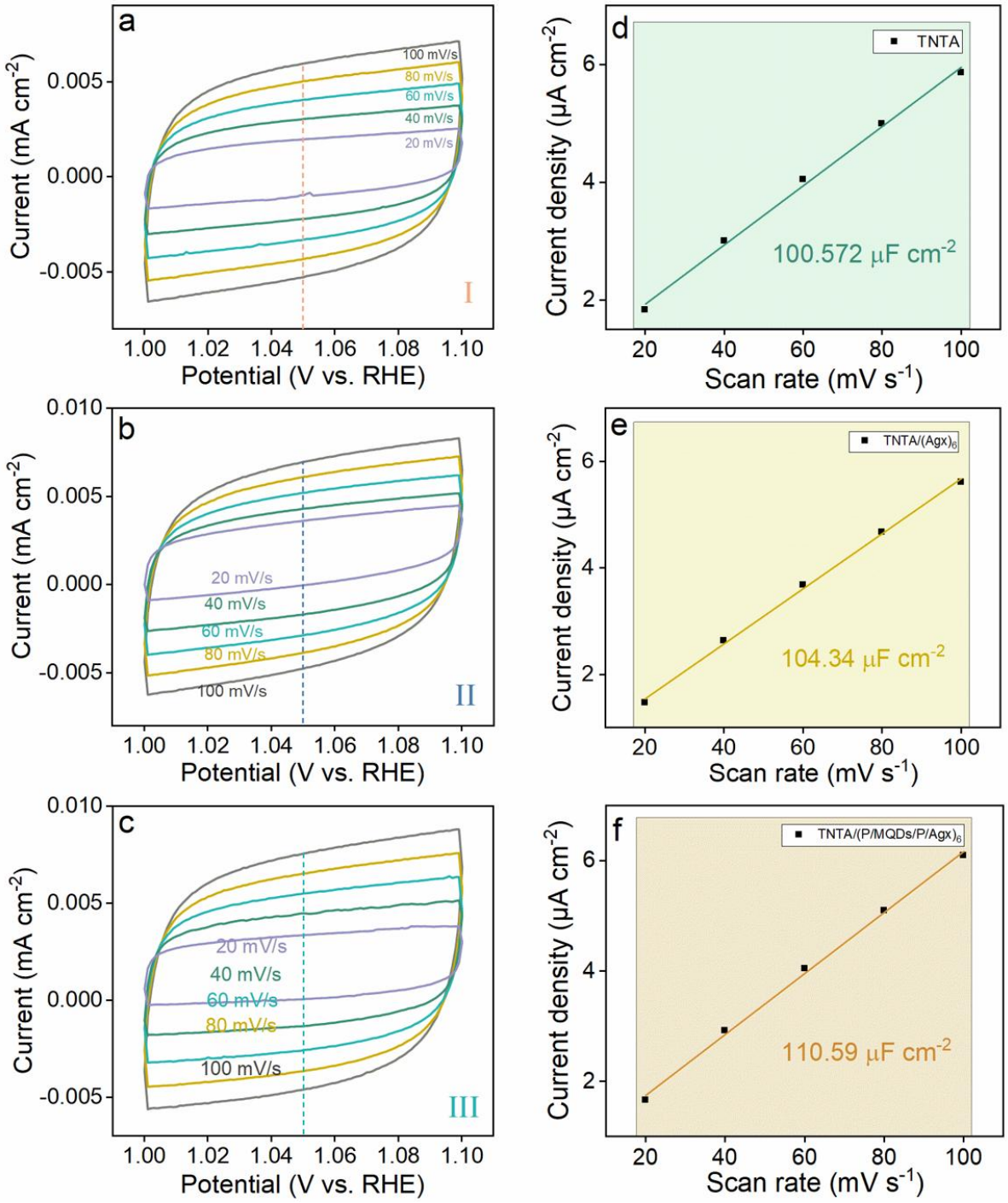

Figure S18. CV plots (1.0-1.1 V vs. RHE) of (a) TNTA, (b) TNTA/$(Ag_x)_6$ and (c) TNTA/$(P/MQDs/P/Ag_x)_6$, along with (d-f) corresponding ESCA results.

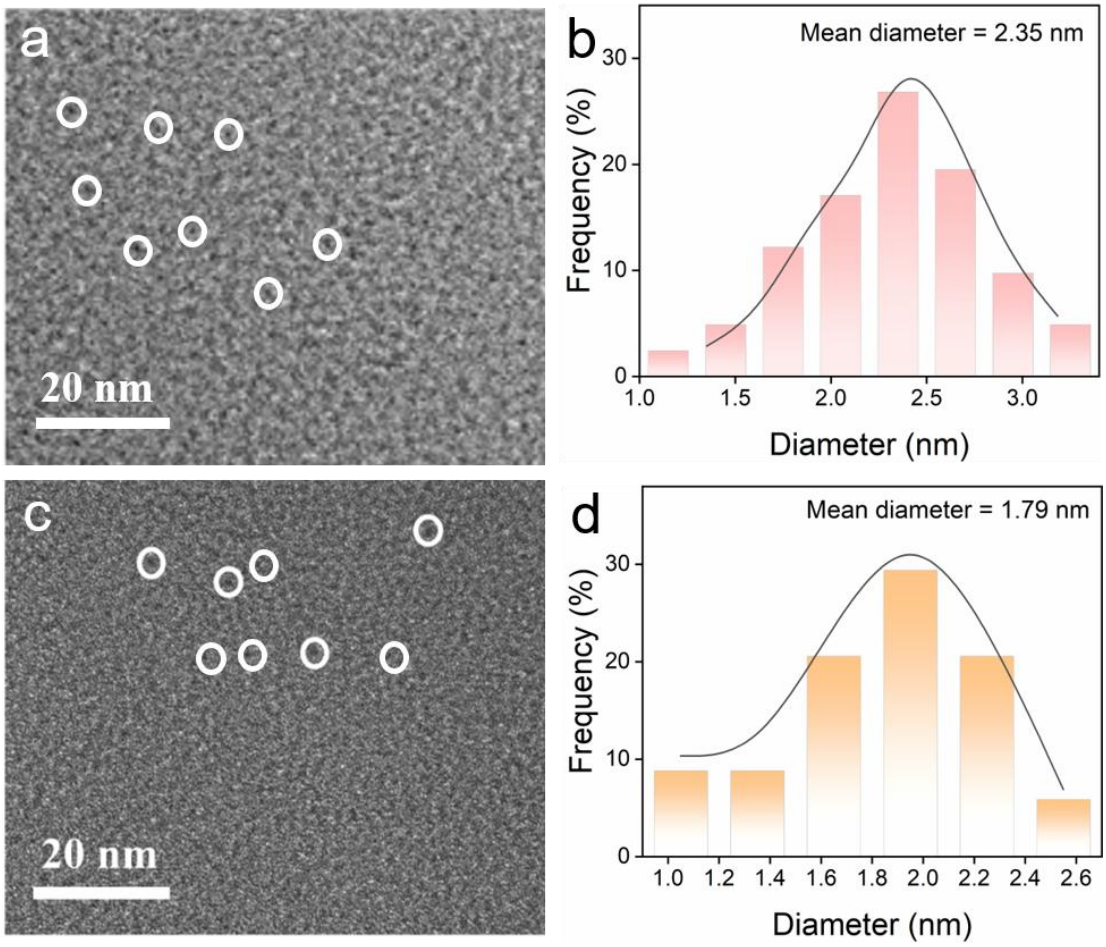

Figure S19. (a) TEM image and (b) size distribution histogram of $Ag_9(GSH)_6$ NCs; (c) TEM image and (d) size distribution histogram of $Ag_{16}(GSH)_9$ NCs.

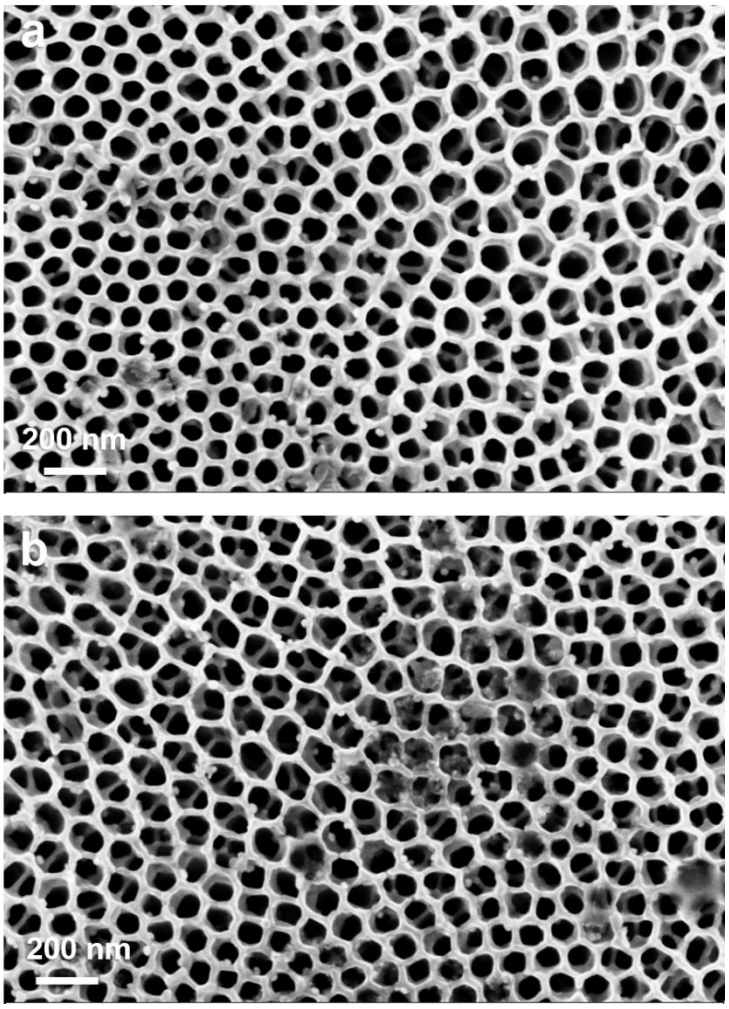

Figure S20. SEM images of (a) TNTA/(P/MQDs/P/Ag_9)$_6$ and (b) TNTA/(P/MQDs/P/Ag_{16})$_6$.

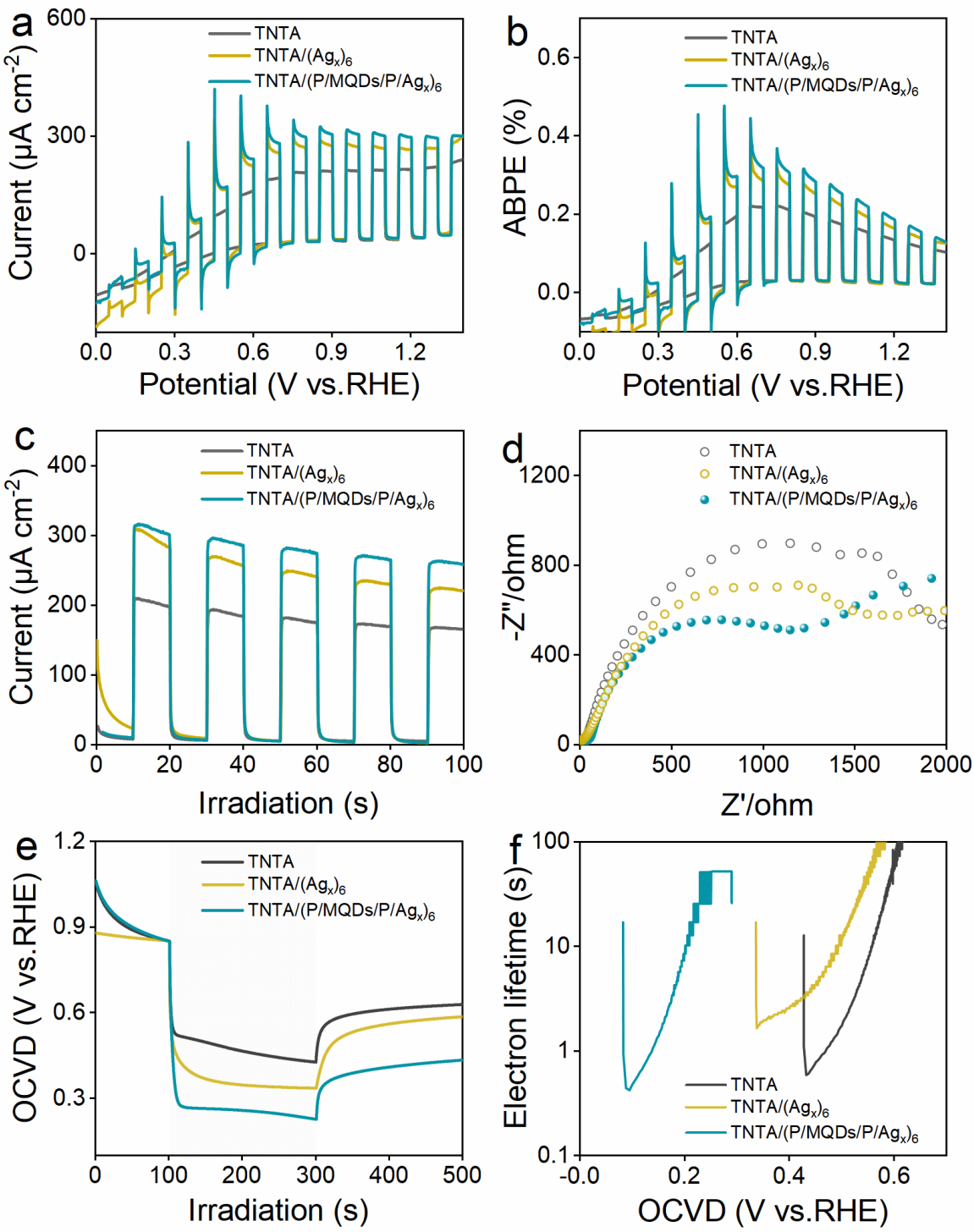

Figure S21. (a) LSV, (b) ABPE, (c) transient photocurrent responses (bias: 1.23 V vs. RHE), (d) EIS, (e) OCVD results, along with (f) electron lifetime for TNTA, TNTA/$(Ag_x)_6$ and TNTA/$(P/MQDs/P/Ag_x)_6$. PEC test conditions: Na_2SO_4 aqueous solution (0.5 M, pH = 7) is utilized as the electrolyte under simulated solar light irradiation (AM 1.5G).

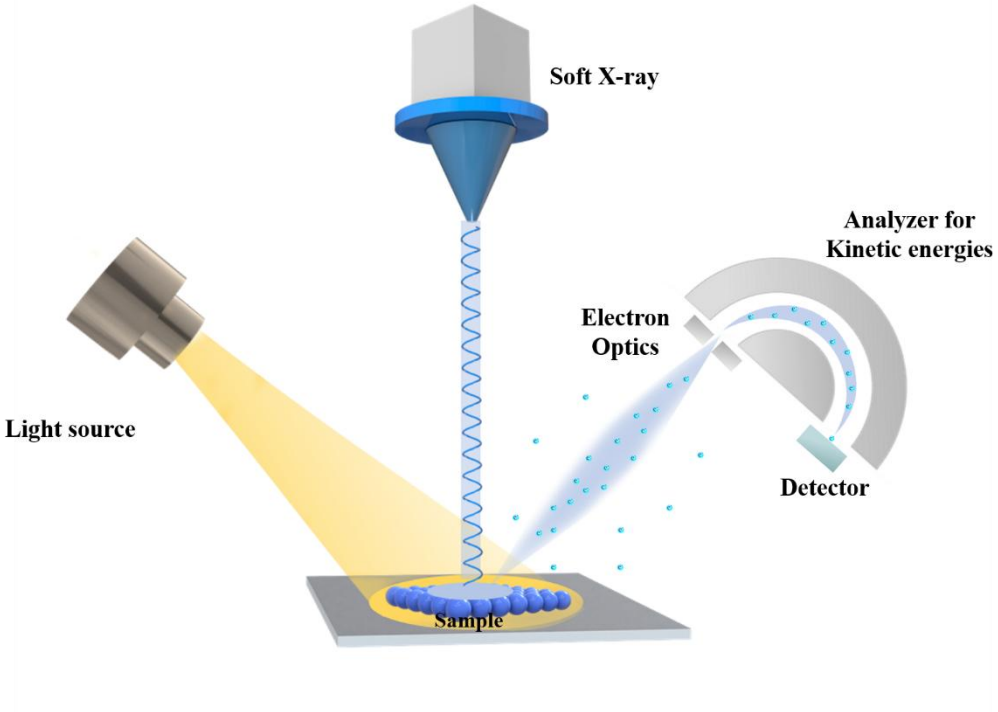

Figure S22. Schematic diagram of in-situ irradiated XPS for probing high-resolution spectra.

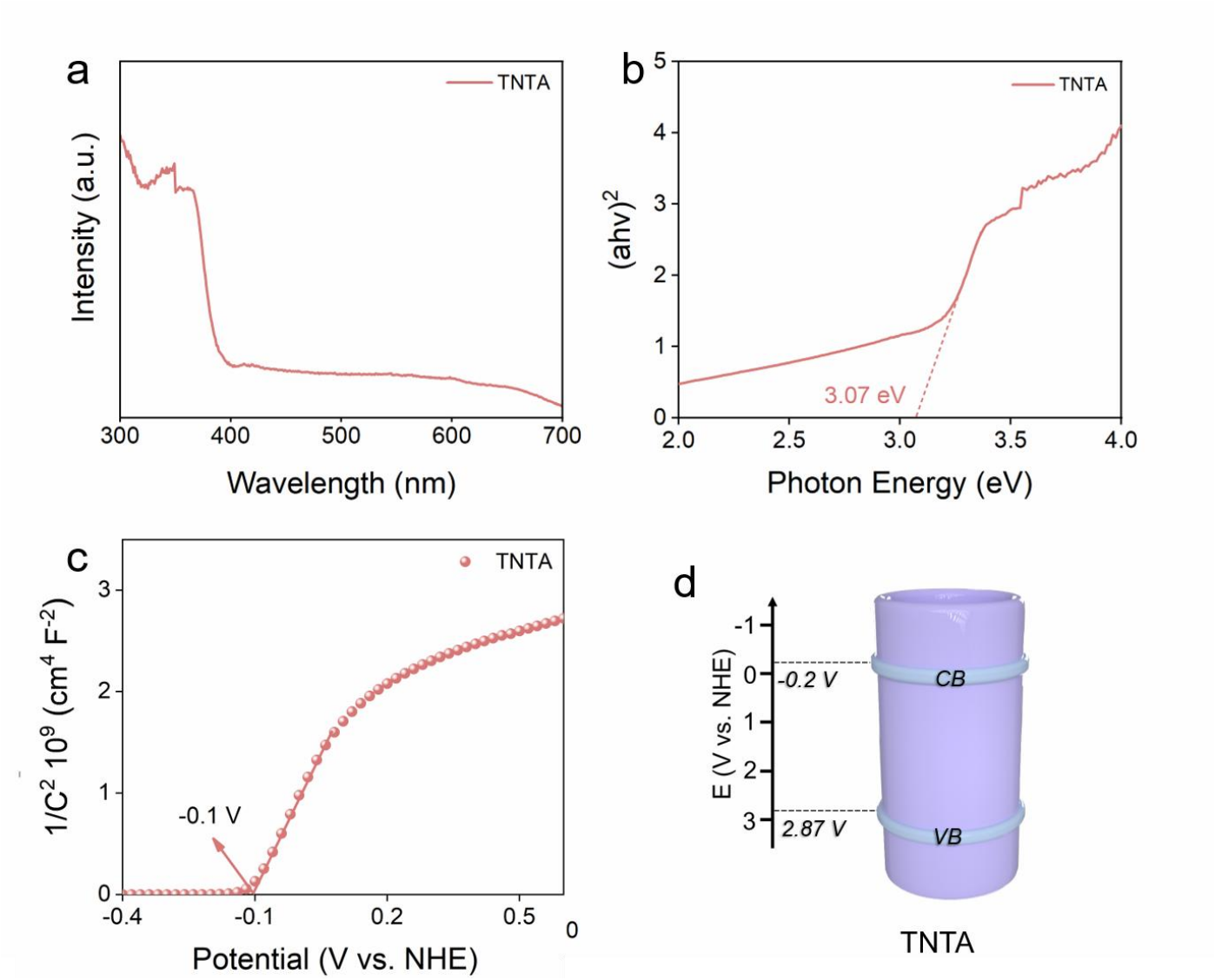

Figure S23. (a) DRS results, (b) bandgap determination, (c) M-S results and (d) schematic diagram showing the energy levels of TiO_2.

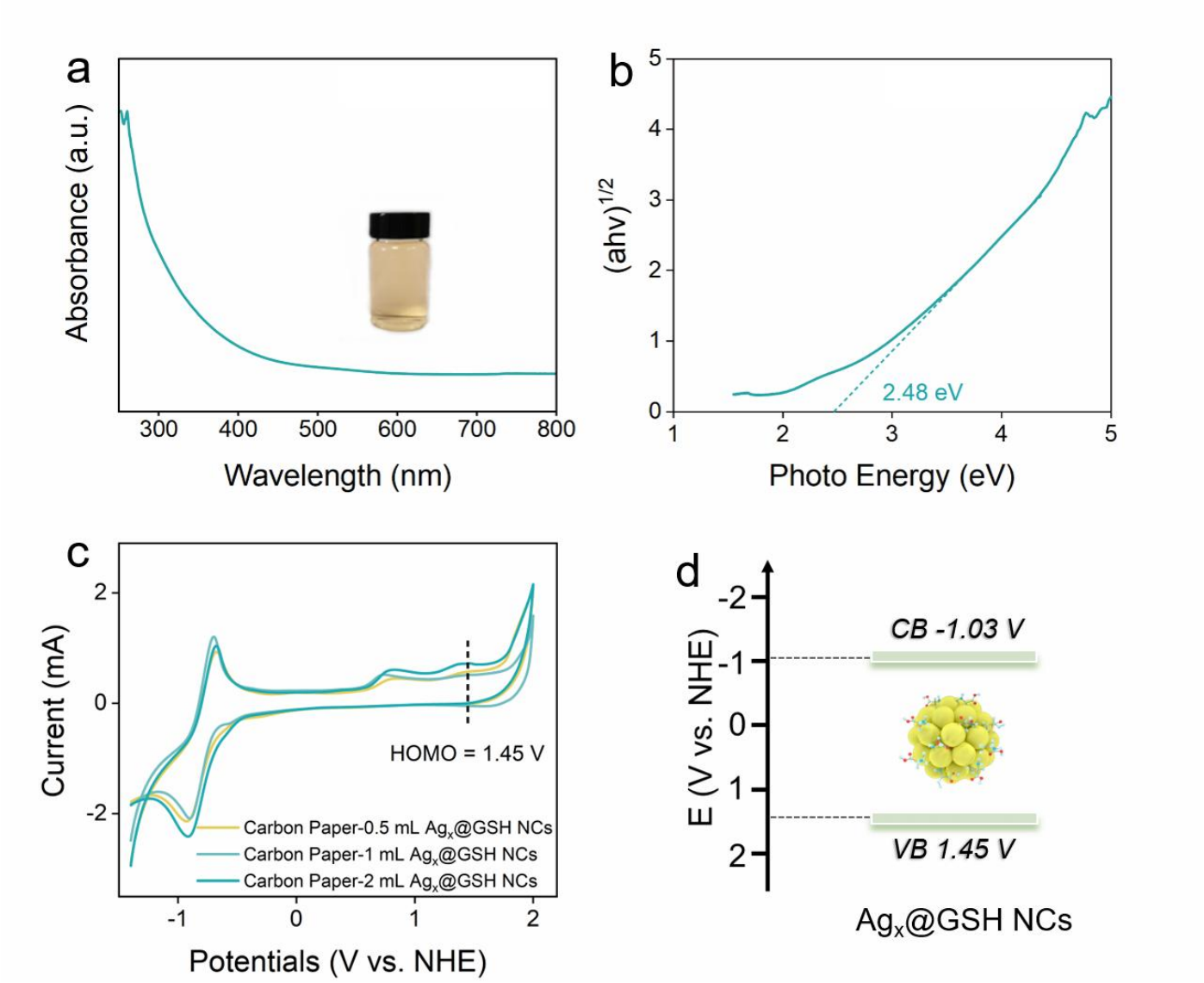

Figure S24. (a) DRS results, (b) bandgap determination, (c) CV results and (d) schematic diagram showing the energy levels of Ag_x@GSH NCs.

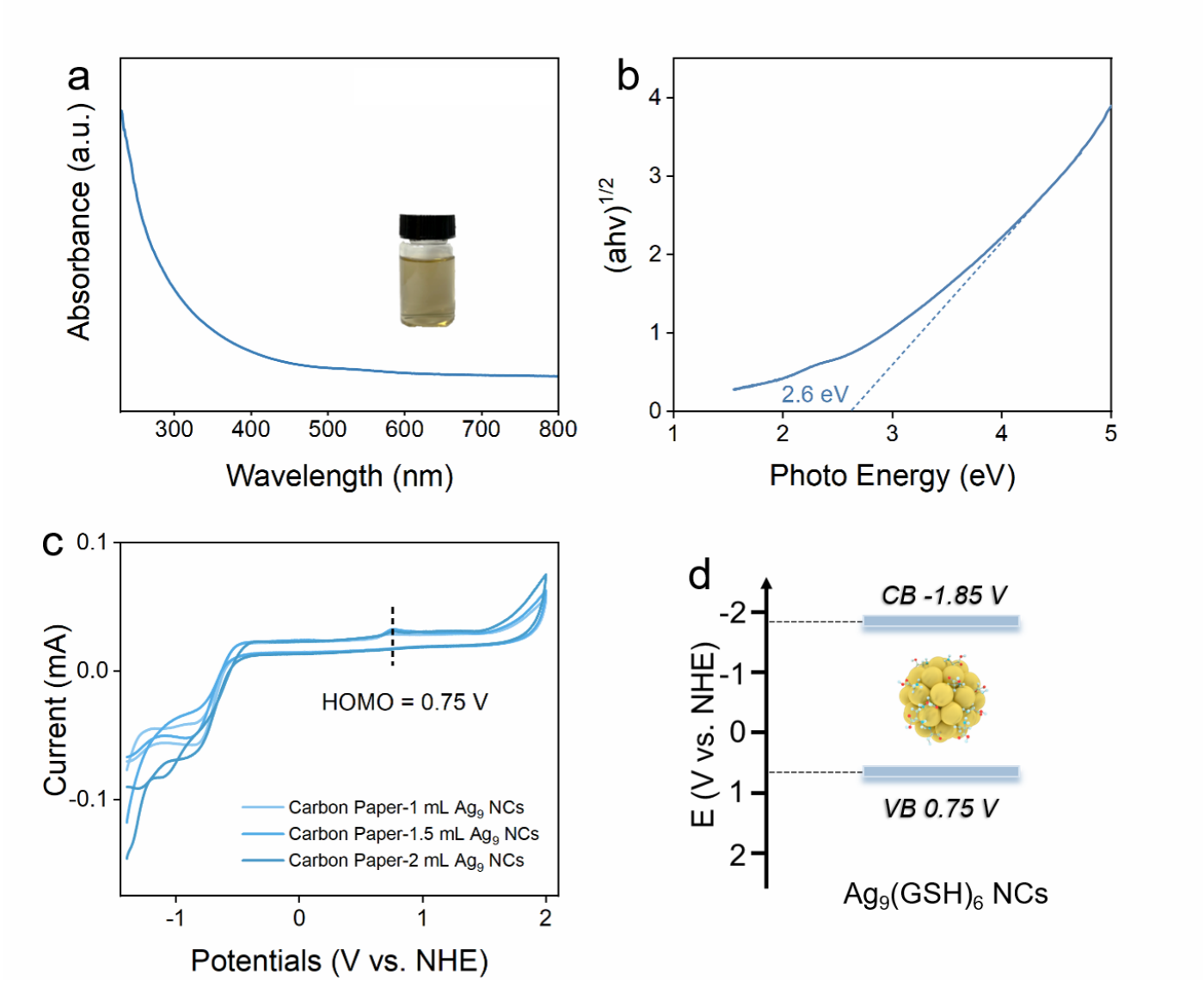

Figure S25. (a) DRS results, (b) bandgap determination, (c) CV results and (d) schematic diagram showing the energy levels of $Ag_9(GSH)_6$ NCs.

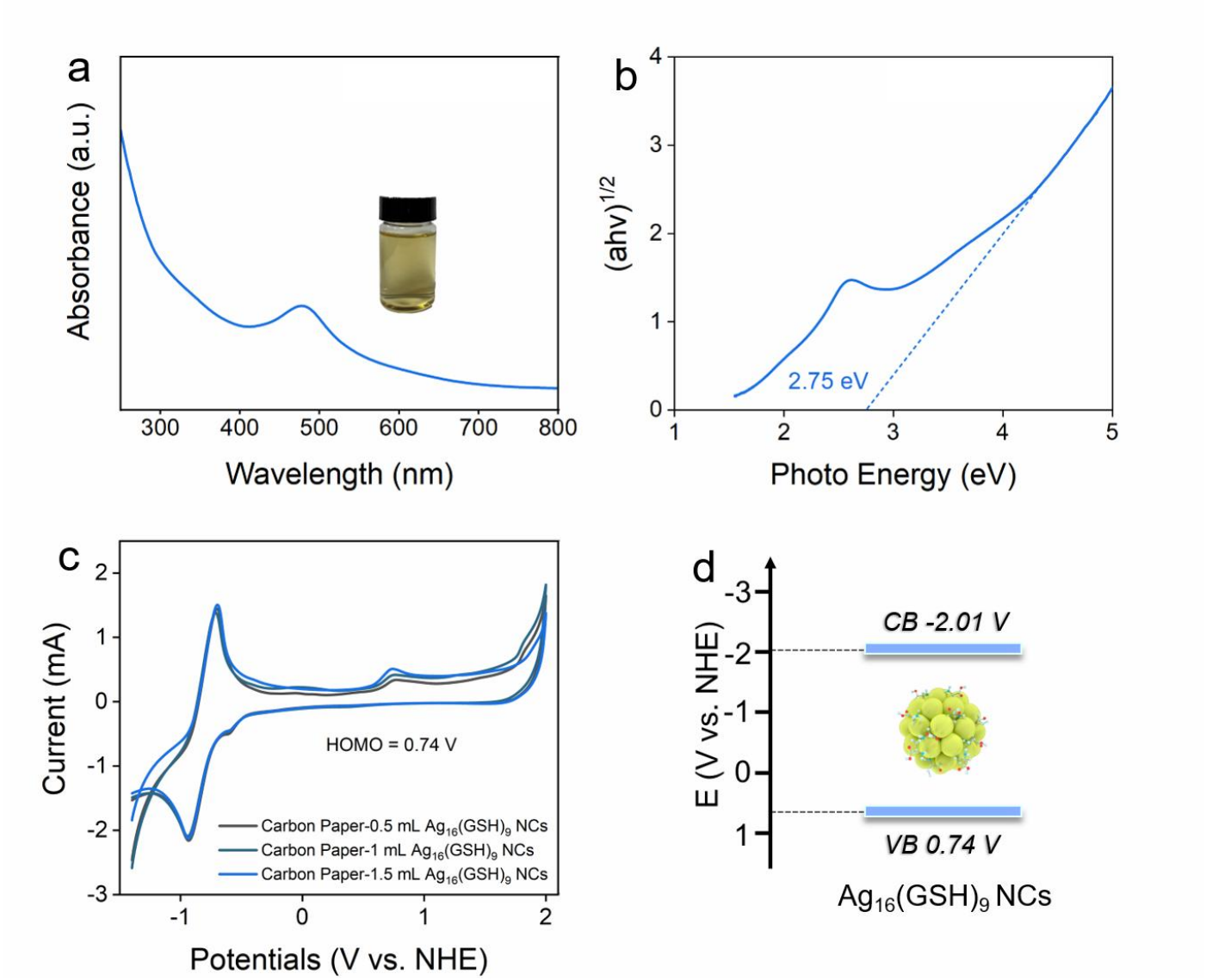

Figure S26. (a) DRS results, (b) bandgap determination, (c) CV results and (d) schematic diagram showing the energy levels of $Ag_{16}(GSH)_9$ NCs.

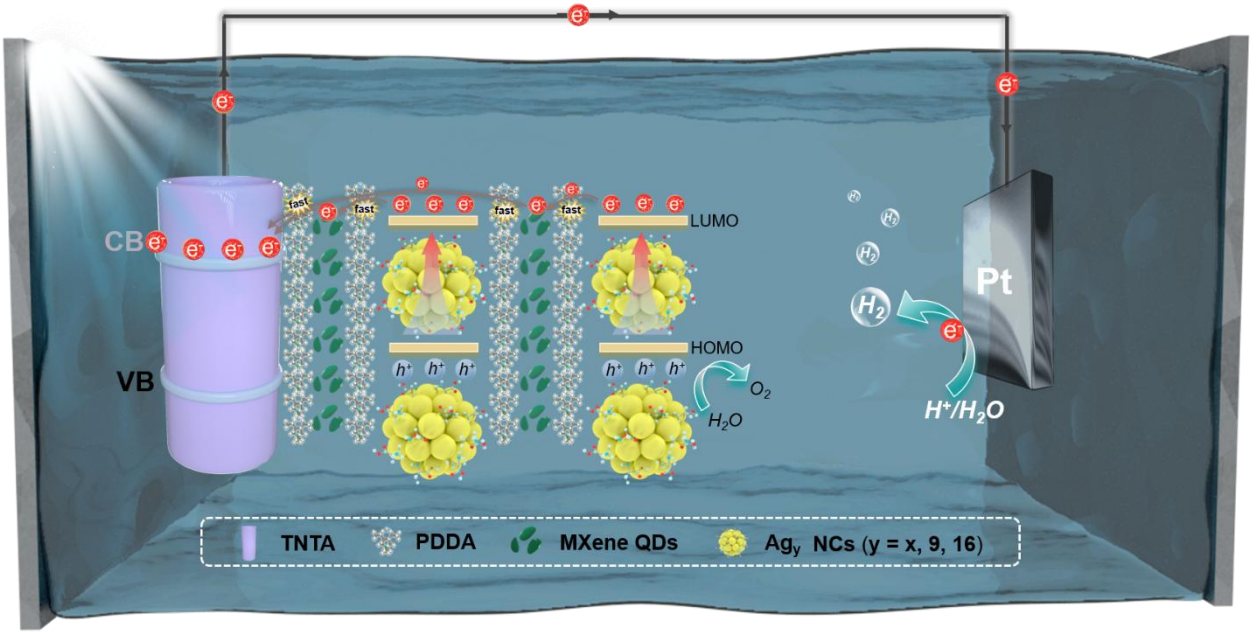

Figure S27. Schematic diagram depicting the PEC water oxidation mechanism of TNTA/(P/MQDs/P/Ag_y)$_n$ photoanodes.

Table S1. Peak position with corresponding functional groups

Peak position	Functional groups	Reference
3430	-OH	[3]
1635	-OH $-NH_2$	[3-5]
1407	-COOH	[6]
1110	Ti-O C-F	[7]

Table S2. Chemical bond species vs. B.E. for different photoelectrodes.

Element	TNTA	TNTA/$(Ag_x)_6$	TNTA/(P/MQDs/P/$Ag_x)_6$	Chemical Bond Species
Ti $2p_{3/2}$	458.65	457.2	458.7	Rutile ($^{4+}$)[8]
Ti $2p_{1/2}$	464.38	462.9	464.4	Rutile ($^{4+}$)[8]
O 1s	529.86	528.5	529.9	Ti-O[9]
O 1s	531.51	530.02	531.6	Ti-OH[9]
C 1s	284.8	284.8	284.8	C-C/C-H[10,11]
C 1s	286.44	286.33	286.4	C-OH[10,11]
C 1s	288.7	288.09	288.29	C=O/C-F[10,11]
N 1s	N．D	N．D	399.82	-NH-/-NH_2[12]
N 1s	N．D	N．D	401.38	NH_4^+[12]
Ag $4f_{5/2}$		83.83	83.94	Ag^0[13]
Ag $4f_{5/2}$		84.46	84.58	Ag^+[2]
Ag $4f_{3/2}$		87.56	87.64	Ag^0[3]
Ag $4f_{3/2}$		88.17	88.3	Ag^+[2]
S $2p_{3/2}$		N．D	161.72	S^{2-}[14]
S $2p_{3/2}$		N．D	164.23	S^{2-}[14]
S $2p_{1/2}$		N．D	162.95	Ag-S[14]

Table S3. Fitted EIS results of photoanodes under visible-light irradiation based on the equivalent circuit.

Photoanodes	**R_s (ohm)**	**R_{ct} (ohm)**	**CPE ($F \cdot cm^{-2}$)**
TNTA	4.979	9456	3.336×10^{-5}
TNTA/$(Ag_x)_6$	36.82	6070	1.005×10^{-3}
TNTA/$(P/MQDs/P/Ag_x)_6$	32.76	1908	3.962×10^{-4}

Table S4. Comparison on the PEC water splitting performances of this work with the previously reported TiO_2-based PEC systems.

Number	*Materials*	*Synthetic method*	*Light source*	*Bias*	*Experimental conditions*	*Photocurrent ($\mu A/cm^2$)*	*Reference*
This work	TNTA/(P/MQDs/P/Ag_x)$_6$	Layer-by-layer assembly	Visible light (λ > 420 nm)	+0.4 V (vs Ag/AgCl)	0.5 M Na_2SO_4	187	/
1	TiO_2-RGO	hydrothermal process	150 mW cm^{-2}	+0.6 V (vs Ag/AgCl)	1 M KOH	55	Sol. Energy, 2019, 190, 185-194.
2	FTO-TiO_2-CPM-121	hydrothermal method	Visible light (λ > 455 nm)	1.23 V (vs RHE)	0.5 M Na_2SO_4	55	Langmuir, 2017, 33, 13634-13639.
3	TiO_2/(CdSe QDs/MQDs)n	Layer-by-layer assembly	Visible light (λ > 420 nm)	+0.4 V (vs Ag/AgCl)	0.5 M Na_2SO_4	105	Small, 2024, 20, 2400958.
4	N-CQDs-decorated TiO_2 NRs	hydrothermal method	Visible light (λ > 420 nm)	0 V (vs Ag/AgCl)	0.1 M phosphate buffered saline	13.89	Chem. Eng. J., 2023, 468, 143583.
5	GOx-CDs/TiO_2 NTAs	hydrothermal process	Visible light (λ > 380 nm)	+0.4 V (vs Ag/AgCl)	0.1 M phosphate buffered saline	50	RSC Adv., 2019, 9, 15084-15091
6	TNBs/CdS NSPs	self-assembly	Visible light (λ > 420 nm)	/	0.1 M Na_2SO_4	13.4	Appl. Catal. A Gen., 2016, 521, 50-56.
7	GQDs-decorated TiO_2 NTs	hydrothermally deposited	Visible light (λ > 400 nm)	0 V (vs Ag/AgCl)	0.1 M phosphate buffered saline	12.96	J. Hazard. Mater., 2022, 426, 128107.
8	$MnFe_2O_4$@SiO_2/TiO_2	hydrothermal method	Visible light (λ > 400 nm)	/	0.1 M Na_2SO_4	40	J. Electroanal. Chem., 2022, 923, 116813.
9	TiO_2 NTA/$AgInS_2$ (3)/In_2S_3(5)-316L	SILAR method	Visible light (λ > 420 nm)	/	3.5% NaCl solution	18	Electrochim. Acta, 2018, 269, 429-440.
10	TiO_2/(PDDA–Ag_x NCs)n	Layer-by-layer assembly	Visible light (λ > 420 nm)	+0.4 V (vs Ag/AgCl)	0.5 M Na_2SO_4	30	J. Mater. Chem. A, 2022,10, 4032-4042.

Table S5. Fitted parameters for time-resolved PL decay spectra of different samples.

Sample	A1(%)	A2(%)	A3(%)	τ_1/ns	τ_1/ns	τ_1/ns
TNTA	49.43	35.15	25.17	0.642	0.914	0.853
TNTA/$(Ag_x)_6$	34.38	38.88	35.71	2.836	3.834	3.601
TNTA/$(P/MQDs/P/Ag_x)_6$	16.19	25.97	39.12	31.757	31.763	31.209

References

[1] J. L. Liu, X. Yan, F. X. Xiao, Alloy Nanoclusters Steering Enhanced Solar Water Oxidation, Inorg. Chem. **2025**, *64*, 13963-13972.

[2] H. Liang, B. J. Liu, B. Tang, S. C. Zhu, S. Li, X. Z. Ge, J. L. Li, J. R. Zhu and F. X. Xiao, Atomically Precise Metal Nanocluster-Mediated Photocatalysis, *ACS Catal.* **2022**, *12*, 4216-4226.

[3] Q. L. Mo, J. L. Li, S. R. Xu, K. Wang, X. Z. Ge, Y. Xiao, G. Wu and F. X. Xiao, Unexpected Insulating Polymer Maneuvered Solar CO_2-to-Syngas Conversion, *Adv. Funct. Mater.* **2022**, *33*, 2210332.

[4] F. X. Xiao and B. Liu, In situ etching-induced self-assembly of metal cluster decorated one-dimensional semiconductors for solar-powered water splitting: unraveling cooperative synergy by photoelectrochemical investigations, *Nanoscale* **2017**, *9*, 17118-17132.

[5] H. Liang, B. J. Liu, B. Tang, S. C. Zhu, S. Li, X. Z. Ge, J. L. Li, J. R. Zhu and F. X. Xiao, Atomically Precise Metal Nanocluster-Mediated Photocatalysis, *ACS Catal.* **2022**, *12*, 4216-4226.

[6] S. H. Xu, T. Gao, X. Y. Feng, Y. N. Mao, P. P. Liu, X. J. Yu and X. L. Luo, Dual ligand co-functionalized fluorescent gold nanoclusters for the "turn on" sensing of glutathione in tumor cells, *J. Mater. Chem. B* **2016**, *4*, 1270-1275.

[7] Z. P. Zeng, Y. B. Yan, J. Chen, P. Zan, Q. H. Tian and P. Chen, Boosting the Photocatalytic Ability of Cu_2O Nanowires for CO_2 Conversion by MXene Quantum Dots, *Adv. Funct. Mater.* **2018**, *29*, 1806500.

[8] Z. B. Li, H. D. Bian, X. F. Xiao, J. D. Shen, C. H. Zhao, J. Lu and Y. Y. Li, Defective Black TiO_2 Nanotube Arrays for Enhanced Photocatalytic and Photoelectrochemical Applications, *ACS Appl. Nano Mater.* **2019**, *2*, 7372-7378.

[9] Y. Xiao, Q. L. Mo, G. Wu, K. Wang, X. Z. Ge, S. R. Xu, J. L. Li, Y. Wu and F. X. Xiao, Charge modulation over atomically precise metal nanoclusters via non-conjugated polymers for photoelectrochemical water oxidation, *J. Mater. Chem. A* **2023**, *11*, 2402-2411.

[10] P. Su, S. Li and F. X. Xiao, Precise Layer-by-Layer Assembly of Dual Quantum Dots Artificial Photosystems Enabling Solar Water Oxidation, *Small* **2024**, *20*, 2400958.

[11] S. Li, Q. L. Mo, S. C. Zhu, Z. Q. Wei, B. Tang, B. J. Liu, H. Liang, Y. Xiao, G. Wu, X. Z. Ge and F. X. Xiao, Unleashing Insulating Polymer as Charge Transport Cascade Mediator, *Adv. Funct. Mater.* **2022**, *32*, 2110848.

[12] S. Y. Wang, D. S. Yu and L. M. Dai, Polyelectrolyte Functionalized Carbon Nanotubes as Efficient Metal-free Electrocatalysts for Oxygen Reduction, *J. Am. Chem. Soc.* **2011**, *133*, 5182-5185.

[13] Z. Q. Wei and F. X. Xiao, Photosensitization Efficiency Modulation of Atomically Precise Silver Nanoclusters for Photoelectrocatalysis, *Inorg. Chem.* **2023**, *62*, 6138-6146.